16th European Signal Processing Conference (EUSIPCO 2008), Lausanne, Switzerland, August 25-29, 2008, copyright by EURASIP

USING PHASE AND MAGNITUDE INFORMATION OF THE COMPLEX DIRECTIONAL FILTER BANK FOR TEXTURE SEGMENTATION

An Vo and Soontorn Oraintara

Department of Electrical Engineering, University of Texas Arlington, TX 76019, USA
E-mail: vpnan@msp.uta.edu, oraintar@uta.edu

ABSTRACT

In this work, a new feature extraction method is proposed for texture segmentation. The approach bases on incorporating the phase information obtained from complex filter banks. The complex directional filter bank (CDFB) is used to decompose a texture image in order to provide complex subband coefficients. The local mean direction, extracted from the phases of the coefficients, is defined as additional features for classification and segmentation. Simulation results show that the CDFB phase information is complementary to the magnitude. Lower classification error rates are achieved. Performance of the proposed method is also compared with other complex filter banks including the Gabor transform and the dual-tree complex wavelet.

1. INTRODUCTION

Texture segmentation is an important application for pattern recognition and image analysis. It has been studied intensively and many different features have been proposed to be used as attributes in segmentation. This paper discusses how magnitude and phase information of the complex directional filter bank (CDFB) [1] coefficients can be used to segment texture images.

One of the common approach in texture segmentation is to use a filter bank to decompose a texture image into subbands [2, 3]. The subband images, after some nonlinear processing, are then used to form local features in segmentation. The Gabor filters are widely used in feature extraction for texture segmentation [4, 5, 6, 7, 8]. In [5], the complex Gabor filters are used to extract features in order to find the boundaries between textures by comparing the channel magnitude responses and detecting discontinuities from large variations in channel phase responses. In [6] a fixed set of Gabor filters are proposed for texture segmentation. The filter selection method is based on reconstruction of the input image from the subband images. Texture classification performances of many different multichannel filtering approaches have been compared in [3], and the conclusion is that no method performs well in all kinds of textures. The wavelet frame [9] and quadrature mirror filter bank (QMF) were two of the best filters. Textures are also characterized by features extracted from images modeled in multiresolution domain as Markov random field [10], hidden Markov tree [11] and coupled Markov random field [12]. Some other works characterize texture by its rotation invariant roughness using fractal dimension [13], adaptive scale fixing [14] and local spectral histogram [15] .

In most of the above segmentation methods, though the phase holds the crucial information about image structures and features [16], only the real part or the magnitude of the transform coefficients is used in texture discrimination. The image features such as edges and shadows are determined by analyzing the phase of the harmonic components [17] or computing the phase congruency [18]. Some other applications exploit the local phase information across scales of the complex wavelet such as the description of image texture [19], the detection of blurred images [20] and object recognition [21]. Another investigation of local phase in the same orientation and the same scale is based on the dual-tree complex wavelet transform [22].

Recently, the complex directional filter bank is proposed for texture image retrieval [23]. When both magnitude and phase information in the complex coefficients are used, the classification system has the best performance compared to other magnitude based methods. The phase information is used successfully in texture image retrieval. In this paper, we discuss how to develop the magnitude and phase based feature extraction method which is proposed in [23] to make it suitable for texture segmentation.

2. COMPLEX DIRECTIONAL FILTER BANK AND LOCAL MEAN DIRECTION FEATURE

2.1 Complex Directional Filter Bank

The shiftable complex directional pyramid is a new image decomposition, which is recently introduced in [1]. The multiresolution filter bank is *shiftable* which means that the energy of the outputs are independent from the position of the input [1]. According to Fig. 1, the very high frequency component of the input is removed to avoid aliasing. The remaining signal is then fed into a multiscale filter bank where the highpass subband is decomposed by two undecimated directional filter banks whose filters satisfy certain phase constraints (see [1] for details). The lowpass subband is decimated by two in both directions before being fed into the next level decomposition, rendering a multiscale representation. At each level, the outputs from the two sets of filters are treated as the real and imaginary parts of complex images. Fig. 1(b) shows the corresponding directional frequency responses of these complex images where, in this example, the number of directions K is set to eight and the number of iterations S is set to three. For more detail of the construction and the properties of the CDFB, the reader is referred to [1].

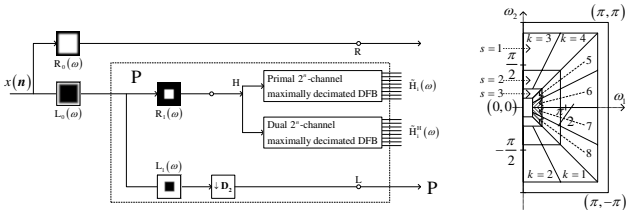

Figure 1: The dual-tree pyramidal directional filter bank for the CDFB: (a) the first iteration (block P) of the pyramid and (b) the corresponding subband index of each subband showing for the case of $K = 8$ directional subbands in $S = 3$ scales.

2.2 Relationship between Local Phase and Feature Orientation

It has been stated in [19] that the local phase varies linearly with the distance from features and in [22] [23], the authors also have observed that the phase of a complex coefficient is consistently linear with respect to the feature offset (distance to the step). However, the proof for this relationship has not been given. Here, we will show that the phase in the vicinity of the feature such as a step or a ramp has a linear relationship with the distance.

Let the input $x(t) = u(t)$ be a unit step signal, and the ideal

complex filter $h(t)$ has one-sided frequency support $H(\omega)$ as:

$$H(\omega) = \begin{cases} 1 & 0 \le \omega_1 \le \omega \le \omega_2, \\ 0 & \text{otherwise.} \end{cases}$$

The output $y(t)$ can be expressed as:

$$\begin{aligned} y(t) &= \frac{1}{2\pi}\int_{-\infty}^{\infty} H(\omega)X(\omega)e^{j\omega t}d\omega = \frac{1}{2\pi}\int_{\omega_1}^{\omega_2}\frac{1}{j\omega}e^{j\omega t}d\omega, \\ &= \frac{1}{2\pi}\int_{\omega_1}^{\omega_2}\frac{1}{j\omega}\sum_{n=0}^{\infty}\frac{(j\omega t)^n}{n!}d\omega, \\ &= \frac{1}{2\pi j}\left(\ln\left|\frac{\omega_2}{\omega_1}\right| + \sum_{n=1}^{\infty}\frac{(jt\omega_2)^n - (jt\omega_1)^n}{n!n}\right). \end{aligned}$$

Because the output $y(t)$ is considered in the vicinity of the step, i.e. $|\omega t| \ll 1$, hence $y(t)$ can be approximated by:

$$y(t) \approx \frac{1}{2\pi j}\left(\ln\left|\frac{\omega_2}{\omega_1}\right| + jt(\omega_2 - \omega_1)\right),$$

and the phase of $y(t)$ can be approximated by:

$$\angle y(t) \approx \tan^{-1}\left(\frac{\omega_2 - \omega_1}{\ln|\frac{\omega_2}{\omega_1}|}t\right) - \frac{\pi}{2} = \tan^{-1}\left(\frac{\omega_2(1-\frac{\omega_1}{\omega_2})}{\ln|(\frac{\omega_1}{\omega_2})^{-1}|}t\right) - \frac{\pi}{2}.$$

Let $p = 1 - \frac{\omega_1}{\omega_2}$. Hence $p \in [0\ 1]$. In addition, we have the inequality: $1 - p \le e^{-p}$ for $0 \le p \le 1$. Therefore,

$$\frac{\omega_2(1-\frac{\omega_1}{\omega_2})t}{\ln|(\frac{\omega_1}{\omega_2})^{-1}|} = \frac{\omega_2 pt}{\ln|(1-p)^{-1}|} \le \frac{\omega_2 pt}{\ln|e^p|} = \omega_2 t \ll 1,$$

and the phase of $y(t)$ can be approximated by:

$$\angle y(t) \approx \left(\frac{\omega_2 - \omega_1}{\ln|\frac{\omega_2}{\omega_1}|}\right)t - \frac{\pi}{2}.$$

Similarly, let the input $x(t) = tu(t)$ be a unit ramp signal and the ideal complex filter $H(\omega)$ be defined as above. In this case, the phase of $y(t)$ can be approximated by:

$$\angle y(t) \approx \tan^{-1}\left(\frac{\omega_1\omega_2\ln|\frac{\omega_2}{\omega_1}|}{\omega_2 - \omega_1}t\right) \approx \left(\frac{\omega_1\omega_2\ln|\frac{\omega_2}{\omega_1}|}{\omega_2 - \omega_1}\right)t.$$

From the above formula, we can see that the phase of $y(t)$ in the vicinity of the features such as the steps or ramps (at $t = 0$) is linear with t (the distance to feature). In the 2-D case, the behavior of the phase is a straight forward extension of the 1-D case.

Let us consider an edge at angle θ_k in the supported region of subband k with $1 \le k \le \frac{K}{4}$. In this case, the center angle of subband γ_k is an acute angle. Assume that the two horizontally adjacent coefficients A and B are located in the neighborhood of an edge as shown in Fig. 3. AA' and BB' represent the distances from A and B to the edge in the direction normal to subband orientation, respectively. The distance between A and B at scale s is $D_s = 2^s$. The phase at A can be estimated by: $\angle y_{sk}(A) = a_{sk}AA' + b_{sk}$. The slope a_{sk} and the intercept b_{sk} are constants for each scale s and orientation k. Therefore the term $(AA' - BB')$ in (2) can be computed from the difference of the phases at A and B:

$$AA' - BB' = \frac{\angle y_{sk}(A) - \angle y_{sk}(B)}{a_{sk}}. \quad (1)$$

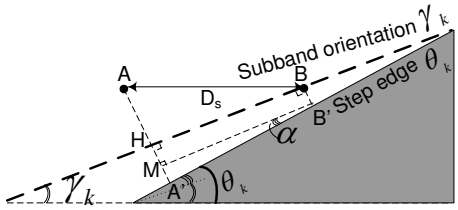

Figure 3: Relationship between the angle θ_k of an edge and the distances from two horizontally adjacent coefficients located at A and B to the edge in the direction normal to the subband orientation k ($1 \le k \le \frac{K}{4}$) at some arbitrary scale.

From Fig. 3 and (1), the feature orientation θ_k of the CDFB subbands can be approximated by [23]

$$\theta_k \approx \gamma_k - \tan\gamma_k + \frac{\angle y_{sk}(A) - \angle y_{sk}(B)}{a_{sk}D_s\cos\gamma_k}. \quad (2)$$

Since the phase difference of two neighboring coefficients or relative phase (RP) can represent a dominant direction θ_k within a directional subband, it is used in the texture image retrieval application. For more details and the cases of other values of k, the reader is referred to [23].

Note that the RP feature proposed in [23] for image retrieval are the circular mean of RPs which determines the global mean direction of the dominant orientations θ_k in the whole subband k and the circular variance determines the measure of global dispersion for these dominant orientations. Since the feature vector [23] represents the global information, we are not able to use this RP feature to discriminate the pixels in the segmentation problem. In the next section, we discuss how to develop the magnitude and phase based feature extraction method to make it suitable for texture segmentation.

2.3 Local Mean Direction for Texture Segmentation

The RP of the CDFB at the spatial location (i, j) of scale s and orientation k is calculated from the corresponding subband coefficients as

$$p_{sk}(i,j) = \begin{cases} \angle y_{sk}(i,j) - \angle y_{sk}(i,j+1) \text{ if } 1 \le k \le \frac{K}{2}, \\ \angle y_{sk}(i,j) - \angle y_{sk}(i+1,j) \text{ if } \frac{K}{2} < k \le K, \end{cases} \quad (3)$$

where $y_{sk}(i,j)$ is the subband complex coefficient at position (i,j), $s = 1,2,...,S$ and $k = 1,2,...,K$. Note that, among the K orientations, the first half ($1 \le k \le \frac{K}{2}$) are more horizontal (vertical in frequency domain) and thus the RP is calculated in the vertical direction whereas the other half ($\frac{K}{2} < k \le K$) are more vertical and it is calculated in the horizontal direction.

Consider when $1 < k \le \frac{K}{4}$. Suppose that there is an edge of angle θ_k at position (i,j). This angle can be estimated from the RP $p_{sk}(i,j)$ by

$$\theta_k \approx \gamma_k - \tan\gamma_k + \frac{p_{sk}(i,j)}{a_{sk}D_s\cos\gamma_k}, \quad (4)$$

where γ_k is the center angle of the subband, and a_{sk} is a constant estimated in the neighborhood of (i,j). In our segmentation algorithm, the RP $p(i,j)$ is replaced by the local mean direction (LMD) of the RPs of the coefficients in the local window, i.e.

$$\theta_k \approx \gamma_k - \tan\gamma_k + \frac{\hat{p}_{sk}(i,j)}{a_{sk}D_s\cos\gamma_k}, \quad (5)$$

where $\hat{p}_{sk}(i,j)$ is the LMD at (i,j) which is defined by

$$\hat{p}_{sk}(i,j) = \arctan\frac{\sum_{i,j\in W}\sin p(i,j)}{\sum_{i,j\in W}\cos p(i,j)}. \quad (6)$$

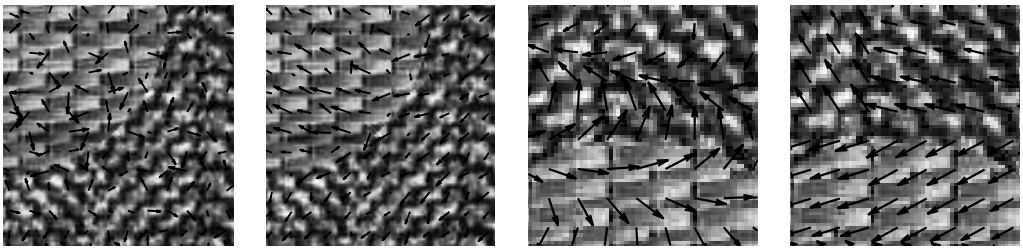

(a) (b) (c) (d)

Figure 2: D17D55 image cropped. (a) CDFB phase ($s = 2, k = 2$), (b) CDFB-LMD ($s = 2, k = 2$), (c) CDFB phase ($s = 5, k = 3$), and (d) CDFB-LMD ($s = 5, k = 3$).

The LMD is also computed by (6) for all other values of k. We can see that the angle of the edge can be estimated from the RP $p_{sk}(i, j)$ in the neighbor of an edge. Hence the RP $p_{sk}(i, j)$ is approximately constant in the vicinity of an edge, and when evaluated in directional subbands, the LMDs can be used to identify the edge direction. The quality of texture segmentation depends on the window size. As the large window is used, the sufficient amount of information is captured. However, a small window is necessary to accurately locate the boundaries between texture regions. This suggests that the selection of window size could possibly be based on the contents of the image. The images with larger texture would require larger window sizes whereas finer textures would require smaller windows. In our experiments, the 5×5 window is used for the texture images and the 3×3 window is used for the real images.

Fig. 2 illustrates the difference between the phase and the LMD. Each image is a combination between two different types of textures (D17 and D55). In Figs. 2(a) and (c), each arrow represents the magnitude (length) and phase (angle) of the CDFB coefficient, while in Figs. 2(b) and (d), the angle represents the estimated angle calculated from the LMDs above. It is clear that the distinction of the LMDs between the two types of textures D17 and D55 can be captured and recognized in Figs. 2(b) and (d) while no clear distinction is obtained from the phase of CDFB coefficients.

Since the LMD determines the local mean direction of the dominant orientations θ_k in the small window, it provides local information of the subband images and can discriminates the pixels. Therefore, the LMD will be used as an additional feature for texture segmentation in the next section.

3. PROPOSED SEGMENTATION METHOD

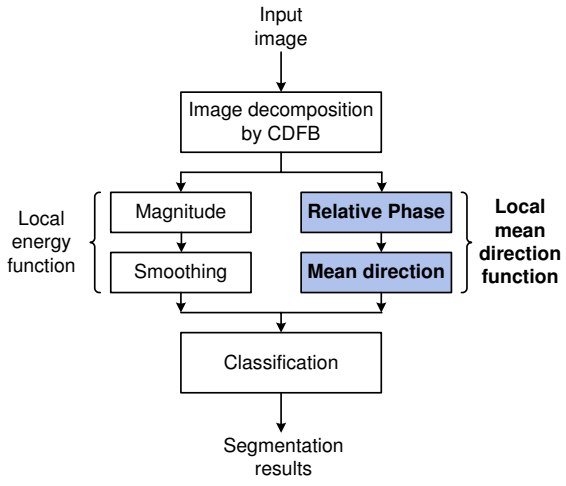

Figure 4: The block diagram for the CDFB-LMD-based segmentation of texture images.

The framework of the proposed method is shown in Fig. 4. A texture image is first decomposed by the CDFB shown in Fig. 1. The complex-valued subband images obtained from the CDFB are then used to extract local magnitude and phase features. For magnitude, a local smoothing window of size $M \times M$ is applied to the magnitude of the complex coefficients. Therefore, each pixel of the output of the window represents an average magnitude of the $M \times M$ block. For phase, a local mean direction at a pixel is determined by the phases of the complex coefficients in the local $M \times M$ block.

The classification is tested on two groups of synthetic texture images from the Brodatz album [24] in our experiments. The texture images used in the first experiment contains fifteen images, each composing of two different types of textures. The second group of textures consists of five images where each has five types of textures. The size of these images is 256×256. For each experiment, each image in the database is decomposed by the following three decomposition methods: the 2-D Gabor transform, the CWT and the CDFB. The numbers of scales and orientations are chosen to give the best results. The Gabor transform is applied with six scales and eight orientations per scale while the CWT has six scales of six orientations (Recall that the number of orientations of the CWT is fixed to six.), and the CDFB has five or six scales of eight orientations.

The local energy is computed over a window by

$$e_k(i, j) = \frac{1}{N} \sum_{(m,n) \in W} w_{mn} |y_k(i-m, j-n)|, \tag{7}$$

where N is the number of elements in the window W. In our experiments, the running average window is used although any other type of windows such as the Gaussian weighted window can also be applied [6]. In texture segmentation, neighboring pixels are very likely to belong to the same texture category. We include the spatial coordinates of the pixel as additional features as proposed in [6] for the five-texture image segmentation. For the case of two-texture image segmentation, the spatial coordinates are not used because the same performance is obtained when adding these two coordinate features. The LMD features of the subbands are estimated by (6).

When using filter banks, the most frequent segmentation method is to search for class prototypes in the feature space by clustering the feature vectors according to certain rules. Each image pixel is classified by determining the class prototype which is closest to its feature vector. In our experiments, we use the standard K-means clustering algorithm used in [9]. Before clustering each feature is normalized to have a zero mean and a constant variance. Some other complex classification methods may also be applied to further improve the segmentation results. However, this is beyond the scope of the paper and might smear the effect of the LMD feature.

4. EXPERIMENT RESULTS

Table 1 summarizes classification error rates using different directional transforms for the fifteen two-texture images. The average

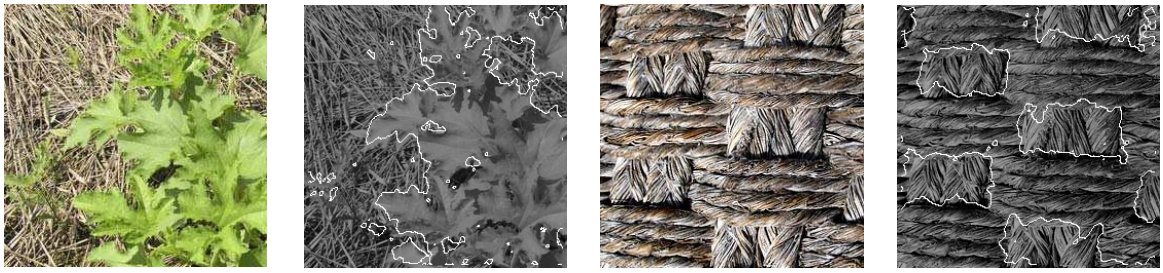

(a) (b) (c) (d)

Figure 5: Segmentation of real images. (a) pumpkinplant image, (c) island texture, (b) and (d) segmentation results using CDFB-LMD

error rates of the methods after using phase are consistently much lower than when using magnitude alone. The combination of CDFB and LMD (CDFB-LMD) yields the best overall segmentation performance of 2.0%. This corresponds to an improvement of 35.4% from using only magnitude. The improvements after phase incorporation for the cases of the Gabor transform (Gabor-LMD) and the CWT (CWT-LMD) are 27.7% and 31.3% respectively.

In the second experiment with five five-texture images, the average classification error rates for the CDFB and CDFB-LMD are summarized in Table 2. The average error rate for the case of CDFB-LMD is 2.6%, much lower than that of the case of CDFB which is 4.7%. In this case, the improvement of the CDFB-LMD after using phase information is 46%. Fig. 5 shows percentage errors of each of the five five-texture images for CDFB and CDFB-LMD. It is evident that the CDFB-LMD yields a nice improvement compared to the CDFB which is based on magnitude information alone. Using this classification result, the segmentation results for the five images are shown in Fig. 6. It is clear that the phase information can complement to magnitude information because higher classification accuracy and better boundaries are achieved. Fig. **??** shows the segmentation results of some real images. The color images are converted to the gray-scale images before segmentation.

Table 1: Comparison of different feature extraction schemes in segmentation of two-texture images

	Gabor/+LMD	**CWT/+LMD**	**CDFB / +LMD**
# scales	6 /6	6 /6	5 /5
# orientations	8 /8	6 /6	8 /8
# features	48 /96	36 /72	40 /80
D21-79	3.3 /2.1	2.8 /2.4	2.7 /1.3
D68-6	2.8 /1.3	3.3 /2.2	1.6 /1.4
D101-106	1.6 /1.4	2.1 /1.6	3.0 /1.6
D12-8	2.3 /2.2	2.7 /2.1	3.5 /2.3
D105-16	1.9 /1.2	1.4 /1.1	2.8 /1.7
D21-57	2.1 /1.9	2.1 /1.7	2.2 /1.4
D103-26	2.6 /2.4	2.0 /1.3	2.7 /2.1
D17-72	2.0 /1.8	3.7 /4.0	2.8 /2.2
D54-56	12.7 /5.6	12.9 /5.4	7.5 /4.8
D21-4	2.5 /2.2	2.9 /2.3	3.2 /1.7
D17-55	1.7 /2.2	3.9 /2.1	4.2 /2.2
D21-77	1.8 /1.2	1.6 /0.7	1.2 /1.0
D73-106	1.1 /1.2	0.8 /0.9	2.2 /2.1
D21-83	3.7 /3.1	3.9 /2.9	4.2 /2.2
D85-11	1.6 /1.6	4.7 /4.2	3.4 /2.5
Ave error	2.9%/2.1%	3.4% /2.3%	3.1% /2.0%
Improvement after using phase	**27.7%**	**31.3%**	**35.4%**

5. CONCLUSION

A new image feature is proposed for texture image segmentation. In addition to magnitude information typically used in many other segmentation methods, phase information is incorporated to further improve the performance. The phase information is extracted from the phase difference of neighboring subband coefficients of the complex transforms including the Gabor transform, the CWT and the CDFB. From the experiments, the segmentation results after using phase are much better ($27.7\% - 46\%$ improvement) than using magnitude alone in term of classification error rate with different texture images. In this paper and the previous work [23], phase information has been *explicitely* and successfully utilized for the applications of texture image segmentation and texture image retrieval. It would be interesting to see if phase information can be beneficial in other image processing applications.

Table 2: Comparison of different feature extraction schemes in segmentation of five-texture images

	Gabor	**CDFB**	**CDFB-LMD**
# scales	6	6	6
# orientations	8	8	8
# features	50	50	98
Ave errors	4.4%	4.7%	2.6%
Improvement			**46.0%**

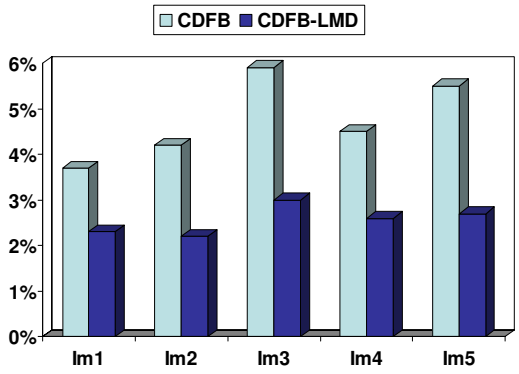

Figure 6: Percentage errors for CDFB and CDFB-LMD in segmentation of five-texture images.

REFERENCES

[1] T.T. Nguyen and S. Oraintara, "The shiftable complex directional pyramid, part 1: Theoretical aspects," *Accepted for publication in the IEEE Transaction on Signal Processing*, Sep 2007.

[2] T. Randen and J.H. Husøy, "Multichannel filtering for image texture segmentation," *Optical Engineering*, vol. 33, no. 8, pp. 2617–2625, August 1994.

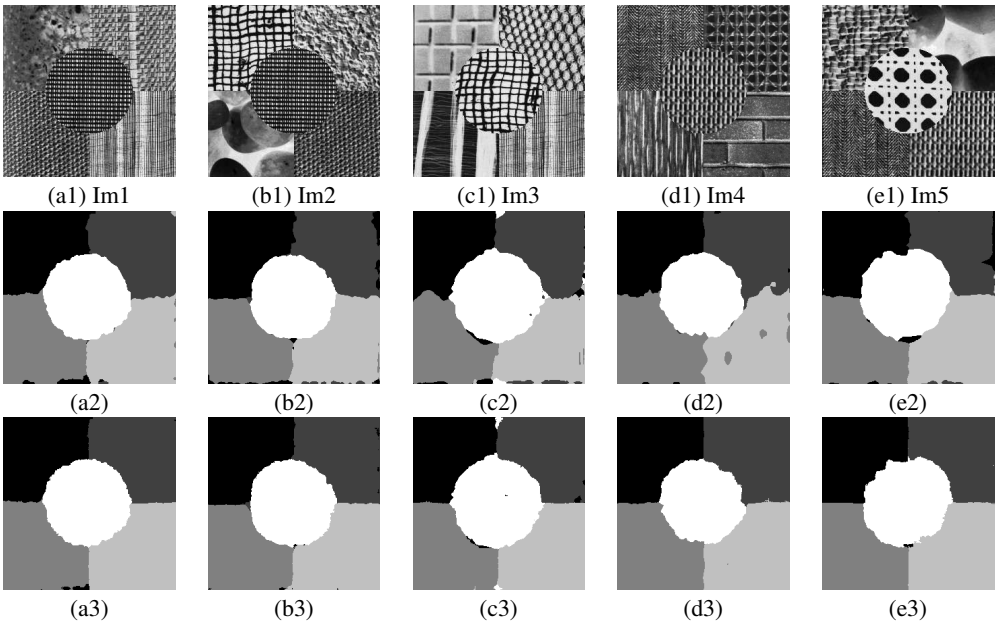

Figure 7: Segmentation of five-texture images. (a1)-(e1): the 256×256 synthetic images from Brodatz album; (a1) Im1 image composed of D73, D85, D77, D106 and D21; (b1) Im2: D104, D4, D30, D77 and D21; (c1) Im3: D1, D36, D51, D106 and D104; (d1) Im4: D16, D52, D68, D94 and D53; (e1) Im5: D84, D30, D16, D53 and D101. (a2)-(e2): segmentation results using CDFB. (a3)-(e3): segmentation results using CDFB-LMD.

[3] T. Randen and J.H. Husøy, "Filtering for texture classification: A comparative study," *IEEE Trans. on PAMI*, vol. 21, no. 4, pp. 291–310, Apr 1999.

[4] A.K. Jain and F. Farrokhnia, "Unsupervised texture segmentation using Gabor filters," in *Proc. IEEE International Conference on Systems, Man and Cybernetics*, Nov 1990, vol. 4-7, pp. 14 – 19.

[5] A.C. Bovik, M. Clark, and W.S. Geisler, "Multichannel texture analysis using localized spatial filters," *IEEE Trans. on Pattern Analysis and Machine Intelligence*, vol. 12, no. 1, pp. 55 – 73, Jan 1990.

[6] A.K. Jain and F. Farrokhnia, "Unsupervised texture segmentation using Gabor filters," *Pattern Recognition*, vol. 24, no. 12, pp. 1167–1186, 1991.

[7] D. Dunn, W.E. Higgins, and J. Wakeley, "Texture segmentation using 2-D Gabor elementary functions," *IEEE Trans. on Pattern Analysis and Machine Intelligence*, vol. 16, no. 2, pp. 130 – 149, Feb. 1994.

[8] D. Dunn and W.E. Higgins, "Optimal Gabor filters for texture segmentation," *IEEE Trans. on Image Processing*, vol. 4, no. 7, pp. 947 – 964, July 1995.

[9] M. Unser, "Texture classification and segmentation using wavelet frames," *IEEE Trans. on Image Processing*, vol. 4, no. 11, pp. 1549–1560, Nov 1995.

[10] S. Krishnamachari and R. Chellappa, "Multiresolution gauss-markov random field models for texture segmentation," *Image Processing, IEEE Transactions on*, vol. 6, no. 2, pp. 251 – 267, Feb 1997.

[11] H. Choi and R.G. Baraniuk, "Multiscale image segmentation using wavelet-domain hidden markov models," *IEEE Transactions on Image Processing*, vol. 10, no. 9, pp. 1309 – 1321, Sept 2001.

[12] Y. Xia, D. Feng, and R. Zhao;, "Adaptive segmentation of textured images by using the coupled markov random field model," *IEEE Transactions on Image Processing*, vol. 15, no. 11, pp. 3559 – 3566, Nov 2006.

[13] D. Charalampidis and T. Kasparis, "Wavelet-based rotational invariant roughness features for texture classification and segmentation," *IEEE Transactions on Image Processing*, vol. 11, no. 8, pp. 825 – 837, Aug 2002.

[14] K.H Liang and T. Tjahjadi, "Adaptive scale fixing for multiscale texture segmentation," *IEEE Transactions on Image Processing*, vol. 15, no. 1, pp. 249 – 256, Jan 2006.

[15] X. Liu and D. Wang, "Image and texture segmentation using local spectral histograms," *IEEE Transactions on Image Processing*, vol. 15, no. 10, pp. 3066 – 3077, 2006.

[16] A. V. Oppenheim and J. S. Lim, "The importance of phase in signals," in *Proc. of the IEEE*, 1981, vol. 69, pp. 529–541.

[17] M. C. Morrone and R. A. Owens, "Feature detection from local energy," *Pattern Recognition Letters*, vol. 6, no. 5, pp. 303 – 313, Dec 1987.

[18] P. Kovesi, "Image features from phase congruency," *Videre: A Journal of Computer Vision Research*, vol. 1, no. 3, pp. 2–26, Summer 1999.

[19] Javier Portilla and Eero P. Simoncelli, "A parametric texture model based on joint statistics of complex wavelet coefficients," *Int'l Journal of Computer Vision*, vol. 40, no. 1, pp. 49–71, Oct 2000.

[20] Z. Wang and E. P. Simoncelli, "Local phase coherence and the perception of blur," in *Advances in Neural Information Processing Systems*, MIT Press, Ed., May 2004, vol. 16.

[21] R. Anderson, N. Kingsbury, and J. Fauqueur, "Coarse-level object recognition using interlevel products of complex wavelets," in *Proc. ICIP*, Sept 2005, vol. 1.

[22] R. Anderson, N. Kingsbury, and J. Fauqueur, "Determining multiscale image feature angles from complex wavelet phases," in *Proc. ICIAR*, Sept 2005.

[23] A.P.N. Vo, S. Oraintara, and T.T. Nguyen, "Using phase and magnitude information of the complex directional filter bank for texture image retrieval," in *Proc. ICIP*, 2007.

[24] P. Brodatz, *A photographic album for artists and designers*, Dover, New York, 1966.